THE JOURNAL OF PHYSICAL CHEMISTRY C

Article

pubs.acs.org/JPCC

Electron Injection Dynamics from Photoexcited Porphyrin Dyes into SnO_2 and TiO_2 Nanoparticles

Rebecca L. Milot, Gary F. Moore,† Robert H. Crabtree, Gary W. Brudvig,* and Charles A. Schmuttenmaer*

Department of Chemistry, Yale University, 225 Prospect Street, P.O. Box 208107, New Haven, Connecticut 06520-8107, United States

Supporting Information

ABSTRACT: The photoexcited electron injection dynamics of free-base and metallo-derivatives of tris(pentafluorophenyl)porphyrins bound to TiO_2 and SnO_2 nanoparticle surfaces have been investigated using time-resolved terahertz spectroscopy (TRTS). The metallo-derivatives include Zn(II), Cu(II), Ni(II), and Pd(II). For the TiO_2–porphyrin assemblies, electron injection from the photoexcited dye to the semiconductor occurs only when using the zinc derivative as the sensitizer because it is the only dye studied in this report with long-lived excited states higher in energy than the TiO_2 conduction band edge. All of the dyes, however, have excited-state energies above the SnO_2 conduction band edge, and the electron injection rates vary widely from 0.4 to 200 ps depending on the sensitizer. For the SnO_2–porphyrin assemblies, electron injection is strongly influenced by competition with alternate deactivation routes that are accessible following Soret band excitation. These results offer thermodynamic and kinetic considerations for designing improved high-potential porphyrin photoanodes with applications to solar-powered water oxidation.

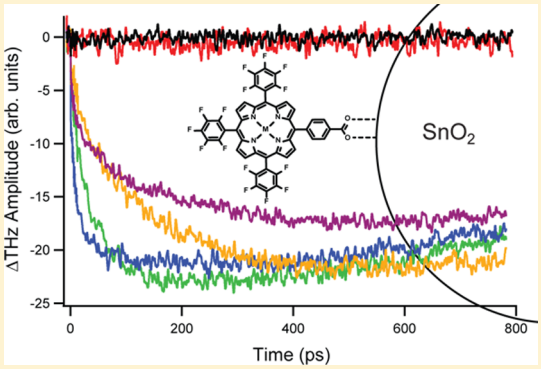

INTRODUCTION

Solar energy has been widely investigated as a renewable alternative to fossil fuels, and significant progress has been made in the area of solar-to-electric transduction using traditional photovoltaic solar cells as well as dye-sensitized solar cells (DSSCs).[1,2] Solar electric cells, however, cannot store energy for future use (i.e., when the sun sets) without utilizing additional components such as batteries or electrolyzers. Biology offers inspiration for achieving integrated solar-to-fuel devices that, like their photosynthetic counterparts, use sunlight to directly oxidize water into oxygen, protons, and electrons (necessary components of fuel production).[3−5] To this aim, researchers have incorporated aspects of DSSCs to construct hybrid water oxidation systems.[6−11] Although their specific design details differ, most of these systems incorporate thin-film dye-sensitized nanoparticle photoanodes to convert visible light to oxidizing power and catalysts to facilitate water oxidation. In general, these systems have relatively low efficiencies and in some cases require the assistance of an external bias voltage or UV illumination.[10]

One approach to improving the efficiency of such devices is identifying the physical processes involved and understanding how they affect each other and the overall performance. In dye-sensitized cells designed for either water oxidation or electricity production, these processes include light harvesting by the sensitizer, electron injection from the sensitizer to the semiconductor, and electron transport through the semiconductor.[10,12] Electron injection plays a particularly important role because it is the step that initiates charge movement. Often, electron injection efficiency can be directly correlated with device performance.[13−18] With femtosecond to picosecond time scales, electron injection has been studied using several ultrafast pump/probe techniques including infrared transient absorption,[19−21] visible transient absorption,[22,23] and THz spectroscopy.[24−28]

The photophysical properties and photoinduced electron-transfer dynamics of porphyrins have been widely studied,[29−32] and porphyrins have also shown success as sensitizers in high efficiency DSSCs.[2,30,33] Accordingly, a series of bis(pentafluorophenyl) sensitizers was recently investigated in the design of photoanodes for DSSCs and photoelectrochemical cells.[6,34] Due to the relatively large potential generated by the porphyrin radical cation/porphyrin redox couple ($P^{\bullet+}$/P), these photoanodes are promising components for water-oxidation systems. This study, which features a selection of analogous 5-(4-carboxyphenyl)-10,15,20-tris-(pentafluorophenyl)porphyrins (Figure 1A) bound to TiO_2 and SnO_2 nanoparticles, analyzes the electron injection from the excited states of the dye molecules to the semiconductor conduction band.

Received: July 8, 2013
Revised: September 20, 2013
Published: September 24, 2013

   dx.doi.org/10.1021/jp406734t | J. Phys. Chem. C 2013, 117, 21662−21670

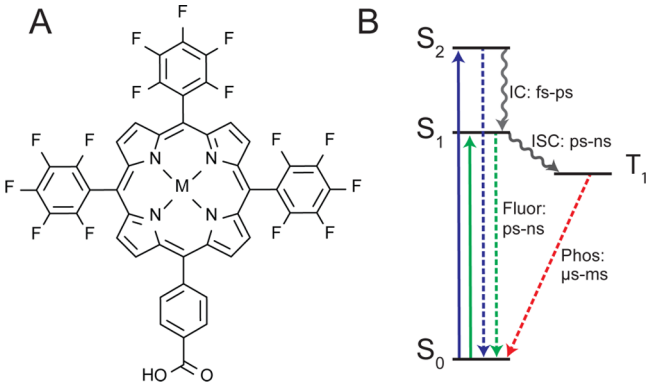

Figure 1. (A) 5-(4-Carboxyphenyl)-10,15,20-tris(pentafluorophenyl)-porphyrin: the porphyrin base (PF_{15}) for the compounds investigated. In this work, M = H_2, Zn(II), Cu(II), Ni(II), or Pd(II). The carboxylic acid functional group serves as an anchor to metal oxide surfaces. (B) Jablonski diagram of a typical porphyrin. Solid lines indicate excitation, dashed lines denote emission, and curvy lines are non-radiative processes. Ranges of typical time scales for internal conversion (IC), intersystem crossing (ISC), fluorescence (Fluor), and phosphorescence (Phos) are indicated.

EXPERIMENTAL METHODS

Synthesis and Characterization. All compounds were synthesized from commercially available starting materials. All chemicals were purchased from Aldrich or Alfa Aesar, and solvents were obtained from Aldrich or Mallinckrodt. Dichloromethane was purified on a 1 m alumina column prior to use (Innovative Technologies, Inc.). All solvents were stored over the appropriate molecular sieves prior to use. The free-base, 5-(4-carboxyphenyl)-10,15,20-tris(pentafluorophenyl)porphyrin (H_2PF_{15}), was prepared using a modified version of a previous report.[35] (See the Supporting Information for synthetic details and characterization.) Zinc, copper, nickel, and palladium ions were inserted into H_2PF_{15} or its methyl ester analogue with metal(II) acetate or chloride salts by standard methods.[36] Thin layer chromatography (TLC) was performed with silica gel coated glass plates from EMD Chemicals. Column chromatography was carried out using silica gel 60, 230−400 mesh, from EMD Chemicals. NMR spectra were recorded on Bruker spectrometers operating at 400 or 500 MHz. Mass spectra were obtained with a matrix-assisted laser desorption/ionization time-of-flight spectrometer (MALDI-TOF). Steady-state absorbance spectra were measured on a Varian Cary 3E UV−visible (UV−vis) spectrophotometer, and steady-state fluorescence spectra were measured using a FluoroLog-3 spectrofluorimeter from Horiba Scientific.

Sample Preparation. TiO_2 nanoparticles (Aeroxide P25) were acquired from Evonik (formerly Degussa). A mixture of 70% anatase and 30% rutile was used, and the particles were 21 nm in diameter on average.[37] SnO_2 nanoparticles (Nano-Arc) were purchased from Alfa Aesar and ranged in size from 22 to 43 nm. Thin films of TiO_2 and SnO_2 were prepared from aqueous suspensions. Pastes composed of 1.0 g of TiO_2 or 1.1 g of SnO_2 in 2.00 mL of water (Milli-Q) were stirred overnight to obtain a homogeneous dispersion and doctor-bladed onto 1 mm thick fused quartz microscope slides (GM Associates). The resulting films were approximately 10 μm thick. The slides were dried at room temperature and sintered in air at 450 °C for 2 h with a ramp rate of 5 °C/min. The TiO_2 and SnO_2 electrodes were sensitized by soaking in a 0.1 mM solution of the appropriate porphyrin compound in 10% ethanol in dichloromethane overnight at room temperature. Following sensitization, the photoanodes were rinsed with 10% ethanol in dichloromethane solution and dried at room temperature. Films of TiO_2 and SnO_2 nanoparticles were highly scattering so spectra were obtained in diffuse reflectance geometry using an integrating sphere. The same samples were used for both the THz and UV−vis measurements.

Electrochemistry. Cyclic voltammetry was performed with an EG&G Princeton Applied Research model 273 potentiostat/galvanostat using a glassy carbon (3 mm diameter) or platinum disc (1.6 mm diameter) working electrode, a platinum counter electrode, and a silver wire pseudoreference electrode in a conventional three-electrode cell. Anhydrous dichloromethane was used as the solvent for electrochemical measurements. The supporting electrolyte was tetrabutylammonium hexafluorophosphate in dichloromethane, and the solution was deoxygenated by bubbling with nitrogen. The working electrode was cleaned between experiments by polishing with an alumina slurry, followed by solvent rinses. The voltammograms of the porphyrin solutions were recorded as the methyl ester analogues for the free-base, zinc, and palladium compounds. The potential of the pseudoreference electrode was determined using the ferrocenium/ferrocene couple as an internal standard (with $E_{1/2}$ taken as 0.690 V vs NHE in dichloromethane).[38] The voltammograms were recorded at a scan rate of 100 mV/s. All potentials listed in this manuscript are referenced to the normal hydrogen electrode (NHE).

Time-Resolved THz Spectroscopy. An amplified Ti:sapphire laser (Tsunami/Spitfire from Spectra Physics) produced 800 mW of pulsed near-IR light at a 1 kHz repetition rate with a ∼120 fs pulse width and 800 nm center wavelength. Roughly two-thirds of the power was frequency doubled and filtered to produce 40 mW of 400 nm (3.10 eV) light for the pump (photoexcitation) beam. The remaining third of the near-IR light was used to generate and detect THz radiation. THz radiation was generated using optical rectification in a ZnTe(110) crystal and detected using free space electro-optic sampling in a second ZnTe(110) crystal. Data were taken at room temperature, and the average of two samples was determined for each data set. To analyze electron injection dynamics, the change in peak time-domain THz transmission was monitored as the time delay between the 400 nm pump pulse and the THz probe pulse was varied. More detailed information on the spectrometer and technique has been reported in the literature.[24,25,39,40]

RESULTS AND DISCUSSION

Steady-State Optical Studies. Porphyrins generally have two main absorption bands in the visible region. A Jablonski diagram showing the relevant transitions is shown in Figure 1B. Excitations from the ground state (S_0) to the first singlet-excited state (S_1) comprise the Q-band. The higher energy Soret band, or B-band, results from excitations from S_0 to S_2. Both of these transitions are $\pi-\pi^*$ transitions that involve electron redistribution within the conjugated π systems of the porphyrin rings.

UV−vis spectra of the H_2PF_{15} ethyl ester in dichloromethane and of the H_2PF_{15} acid on TiO_2 as well as SnO_2 surfaces are shown in Figure 2. Peak positions for all of the porphyrins are listed in Table 1, and additional spectra can be found in Figure S1 (Supporting Information). The two peaks (four for H_2PF_{15}) observed between 500 and 600 nm form the Q-band. The Soret bands, or B-bands, are observed in the 400−420 nm range. The

dx.doi.org/10.1021/jp406734t | J. Phys. Chem. C 2013, 117, 21662−21670

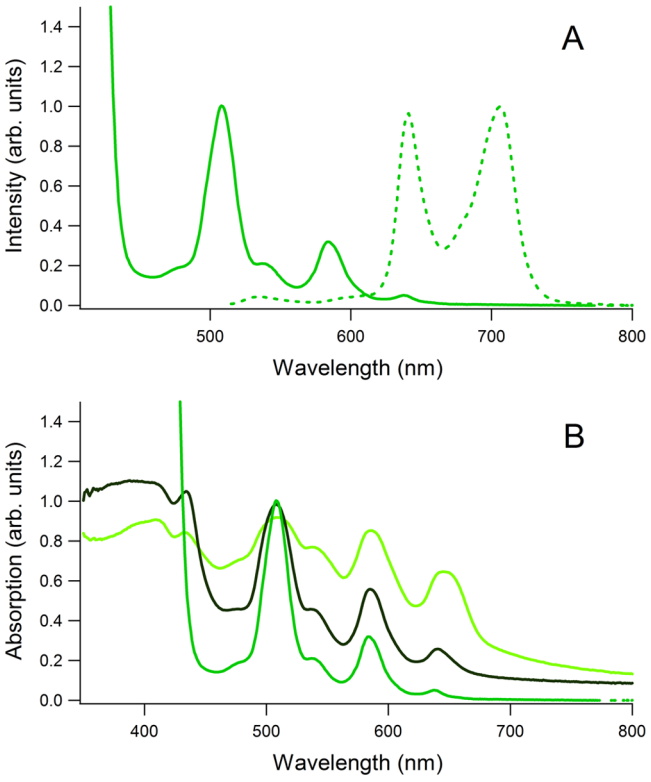

Figure 2. Steady-state absorption and emission spectra for H_2PF_{15}. (A) Normalized absorption (solid line) and emission (dashed line) spectra of H_2PF_{15} methyl ester in dichloromethane. (B) Absorption spectra for H_2PF_{15} methyl ester in dichloromethane (medium green), for H_2PF_{15} on the TiO_2 surface (light green), and for H_2PF_{15} on the SnO_2 surface (dark green).

Q-band peaks for the porphyrins bound to TiO_2 and SnO_2 are broadened in relation to the peaks in dichloromethane but are not significantly red-shifted, which suggests little to no surface aggregation.[41]

All porphyrins studied in this report except for $NiPF_{15}$ exhibit visible emission upon illumination. The emission spectrum of H_2PF_{15} is shown in Figure 2A, emission maxima for all of the porphyrins are listed in Table 1, and all emission spectra are included in Figure S1. As proposed by Gouterman, porphyrins can be classified as fluorescent, phosphorescent, luminescent, or radiationless based on their emission properties.[31] Furthermore, the best predictor of emission properties is the identity of the central substituent (metal ion) of the porphyrin ring. Figure 1B shows schematically the various radiative and non-radiative processes that can occur in porphyrins after either Soret or Q-band excitation.

Porphyrins that show emission primarily from the S_1 state are classified as fluorescent. The emission spectra of H_2PF_{15} and $ZnPF_{15}$ are characteristic of fluorescence (Figures 1A and S1) and exhibit two strong peaks, Q(0,0) and Q(0,1).

Phosphorescent porphyrins undergo rapid intersystem crossing from the S_1 state to the lowest-lying triplet state T_1, from which emission occurs. Fluorescence may still occur from the S_1 state but with decreased quantum yield relative to fluorescent porphyrins.[31] Palladium porphyrins are typically phosphorescent because the heavy Pd(II) cation increases spin−orbit coupling, which increases the rate of intersystem crossing from S_1 to T_1. The weak fluorescence observed for $PdPF_{15}$ versus H_2PF_{15} and $ZnPF_{15}$ (Figure S2) is characteristic of phosphorescent porphyrins.

The emission from luminescent porphyrins is neither purely fluorescent nor phosphorescent due to mixing of triplet and singlet states. In 1968, Gouterman coined the terms "tripdoublet" and "tripquartet" to describe the mixed states that arise when a paramagnetic metal with one unpaired electron, such as Cu(II), is coordinated by a porphyrin.[42] This terminology has been extended to "singdoublets" as well. Since the coupling is fairly weak, the terminology retains the triplet or singlet identity of the underlying porphyrin state. However, it is necessary to acknowledge mixing of the unpaired electron from Cu(II), thereby resulting in triplet states becoming tripdoublets (^{2}T) or tripquartets (^{4}T), while singlet states become singdoublets (^{2}S). The emission of $CuPF_{15}$, which has one broad peak with a maximum value of 706 nm, is consistent with the luminescence reported in the literature for similar Cu porphyrins.[43,44]

Porphyrins that yield no detectable photoluminescence upon excitation, due to the availability of rapid relaxation pathways, are termed radiationless. In the well-documented case of Ni porphyrins, these relaxation pathways involve metal centered (d, d) states, which are accessible because of unoccupied d-orbitals on the Ni(II) cation.[29] Accordingly, essentially no emission is observed from $NiPF_{15}$.

Electrochemistry. The pentafluorophenyl groups have a strong influence on the electrochemical properties of the porphyrin ring system, since their electron withdrawing nature destabilizes formation of the radical cation species.[45] For the methyl ester derivative of H_2PF_{15} in dichloromethane, two quasi-reversible one-electron redox processes are observed with midpoint potentials ($E_{1/2}$) of 1.68 and 1.93 V vs NHE. These potentials are significantly shifted in the anodic direction (more

Table 1. Steady-State Optical Properties of PF_{15} Methyl Esters in Dichloromethane

	absorption maxima (nm, eV)			emission maxima (nm, eV)	
porphyrin	B(0,0)	Q(1,0)[a]	Q(0,0)[a]	Q(0,0)[a]	Q(0,1)[a]
H_2PF_{15}	413, *3.01*	507, *2.45*[b]	536, *2.31*[b]	641, *1.93*	706, *1.76*
		583, *2.13*[b]	637, *1.95*[b]		
$ZnPF_{15}$	415, *2.99*	544, *2.28*	578, *2.15*	585, *2.12*	637, *1.95*
$CuPF_{15}$	409, *3.03*	535, *2.32*	570, *2.18*		706, *1.76*[c]
$NiPF_{15}$	406, *3.05*	524, *2.37*	557, *2.22*		
$PdPF_{15}$	410, *3.02*	520, *2.38*	553, *2.24*	561, *2.21*	604, *2.05*

[a]In this notation, the numbers in parentheses are the number of vibrational quanta in the excited and ground electronic states, respectively. [b]Due to the reduced symmetry of H_2PF_{15} relative to its metalated counterparts, the Q(0,0) peak is split into $Q_x(0,0)$ and $Q_y(0,0)$ peaks and Q(1,0) is split into $Q_x(1,0)$ and $Q_y(1,0)$. The Q_y peaks are observed at shorter wavelengths (higher energies). [c]The emission peak observed for $CuPF_{15}$ is better classified as a T(0,0) peak because it represents emission from the tripdoublet−quartet manifold.[29]

dx.doi.org/10.1021/jp406734t | J. Phys. Chem. C 2013, 117, 21662−21670

positive potentials) compared to the bis(pentafluorophenyl)-porphyrin analogue [5,15-*bis*(4-carbomethoxyphenyl)-10,20-bis(pentafluorophenyl)porphyrin], where the porphyrin radical cation/porphyrin couple ($P^{\bullet+}/P$) occurs with an $E_{1/2}$ value of 1.57 V vs NHE,[6,34] and the nonfluorinated analogue [5,15-bis(4-carbomethoxyphenyl)-10,20-bis(2,4,5-trimethylphenyl)-porphyrin], where the $P^{\bullet+}/P$ couple occurs with an $E_{1/2}$ value of 1.29 V vs NHE.[46] For the metallo complexes, the $P^{\bullet+}/P$ couple can be further perturbed anodically or cathodically. The observed potentials for the Zn, Ni, Cu, and Pd species are provided in Table 2.

Table 2. Ground State Reduction Potentials (V vs NHE) of PF_{15} Methyl Esters Determined by Cyclic Voltammetry[a]

porphyrin	$^{I}E_{1/2}$ (V)	ΔE_p[b] (mV)	$^{II}E_{1/2}$ (V)	ΔE_p[b] (mV)
H_2PF_{15}	+1.68	99	+1.93	104
$ZnPF_{15}$	+1.47	131	+1.72	132
$CuPF_{15}$	+1.63	196	+1.96	234
$NiPF_{15}$	+1.68	150		
$PdPF_{15}$	+1.73	136		

[a]The cyclic voltammograms are shown in Figure S3 (Supporting Information). [b]Peak-to-peak separations of the observed couples.

In accordance with the Rehm–Weller approximation,[47,48] excited-state reduction potentials for the S_1 state are estimated by adding the E^{00} transition energies to the corresponding ground state potentials as follows:

$$E^{\circ}(P^{\bullet+}/{}^{1}P) \approx E^{\circ}(P^{\bullet+}/P) - \frac{E^{00}(P \rightarrow {}^{1}P)}{e} \quad (1)$$

where $E^{\circ}(P^{\bullet+}/{}^{1}P)$ is the excited-state potential for the porphyrin-radical cation/singlet state excited porphyrin couple, $E^{\circ}(P^{\bullet+}/P)$ is the ground state potential for the porphyrin-radical cation/porphyrin couple, $E^{00}(P \rightarrow {}^{1}P)$ is the estimated E^{00} porphyrin ground state to porphyrin singlet state transition energy ($S_0 - S_1$ energy difference), and e is the elementary charge of an electron.

In this report, the S_2 state reduction potentials were approximated by adding the energy (in eV) at the Soret band maximum to the ground-state potential for the $P^{\bullet+}/P$ couple. T_1 state energies were estimated in a similar fashion using electrochemical and emission data for meso-tetraphenylporphyrin (TPP) analogues of the PF_{15} porphyrins.[29]

The values of these excited-state reduction potentials (Figure 3 and Table S1) are pertinent because they determine the thermodynamic feasibility of photoinduced electron transfer into the metal oxide conduction band. As seen in Figure 3, all of the S_2 potentials are more negative (higher in energy) than the conduction band edge of both TiO_2 and SnO_2, so electron injection into either material is possible from these states. The potentials of the S_1 states of the PF_{15} compounds are closer to the TiO_2 conduction band edge potential. The $ZnPF_{15}$ potential is 0.09 V negative of the conduction band, whereas the potentials for H_2PF_{15} and $PdPF_{15}$ are 0.250 and 0.08 V positive of it, respectively. The potentials of $CuPF_{15}$ and $NiPF_{15}$ are nearly isoenergetic with the conduction band. As a result, electron injection into TiO_2 from S_1 is expected to occur for $ZnPF_{15}$ only.

For SnO_2, however, the potentials of the S_1 states of the PF_{15} compounds range from 0.2 to 0.6 V negative of the conduction band edge, so electron injection is thermodynamically possible from all of them. Although none of the T_1 states are more

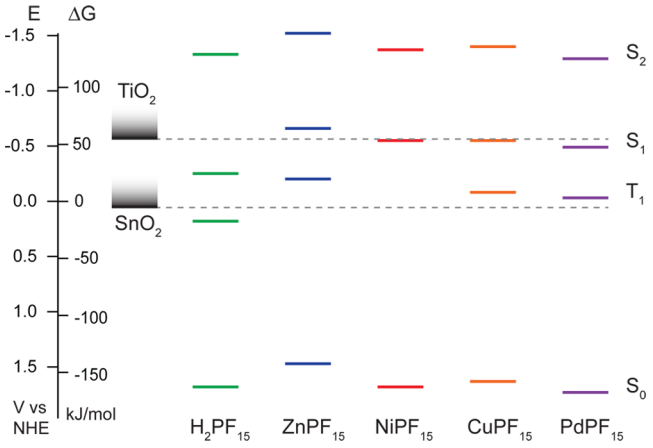

Figure 3. Energy levels relevant to electron injection. Estimates of the S_0, T_1, S_1, and S_2 levels are indicated for the porphyrin sensitizers. For TiO_2 and SnO_2, only the positions of the conduction band edges at neutral pH are shown. Values for all energy levels are provided in Table S1 (Supporting Information).

negative than the TiO_2 conduction band edge, all of them except for H_2PF_{15} are negative of the SnO_2 band edge, indicating that electron injection from T_1 into SnO_2 is possible (except for H_2PF_{15}).

Time-Resolved THz Spectroscopy. Time-Resolved THz Spectroscopy (TRTS) is a proven method for measuring sub-picosecond electron-injection dynamics and efficiency in dye-sensitized nanoparticulate systems.[13,17,24−27,34,49,50] TRTS employs an ultrafast optical pump pulse followed by a THz probe pulse and is unique in that it is a noncontact electrical probe capable of monitoring photoconductivity on a sub-picosecond time scale. Because mobile conduction band electrons alter the transmission of THz radiation, a change in THz amplitude upon photoexcitation is attributable to a change in conductivity. The change in THz amplitude as a function of the pump–probe delay time provides information about both the dynamics and efficiency of electron injection. While arbitrary units for the change in THz transmission are used in Figures 4 and 5, the same arbitrary units are used for all samples studied, and thus, they may be directly compared to each other.

Since conductivity is proportional to the product of the carrier density and carrier mobility,[39,51] TRTS provides a direct measure of electron injection efficiency if the mobility is constant, as is the case with a series of sensitizers all bound to a particular metal oxide. Results from TiO_2 and SnO_2 will therefore be discussed separately, since SnO_2 has a higher mobility than TiO_2.[17]

TiO_2. The electron injection efficiencies and dynamics of the porphyrin dyes bound to TiO_2 nanoparticles are shown in Figure 4. A control sample with no dye (denoted "bare TiO_2") was measured to demonstrate that there is almost no direct carrier generation from either two-photon absorption or excitation from band edge or midgap states. Of all of the porphyrins examined here, only $ZnPF_{15}$ exhibits significant electron injection into TiO_2. $CuPF_{15}$ and H_2PF_{15} show a very small amount of electron injection, and the signals of the $NiPF_{15}$ and $PdPF_{15}$ samples are indistinguishable from that of bare TiO_2.

Electron injection from $ZnPF_{15}$ into TiO_2 occurs faster than the ~400 fs time resolution of the TRTS setup.[39,40] This time

dx.doi.org/10.1021/jp406734t | J. Phys. Chem. C 2013, 117, 21662−21670

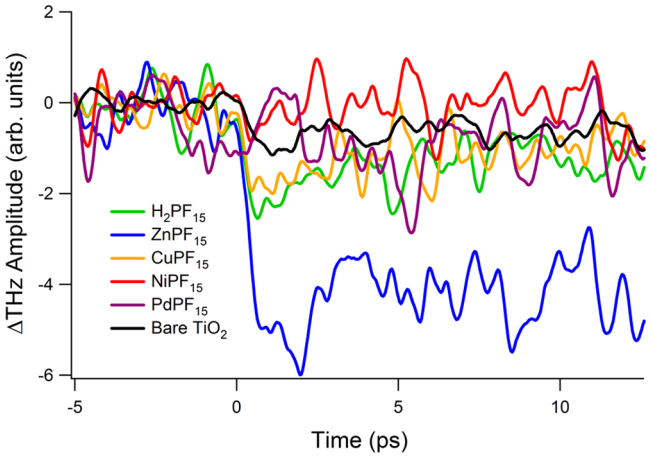

Figure 4. Electron injection dynamics into TiO_2 with 400 nm excitation as observed by TRTS. A more negative change in THz amplitude indicates more efficient electron injection. Zero on the time axis corresponds to the arrival of the pump pulse.

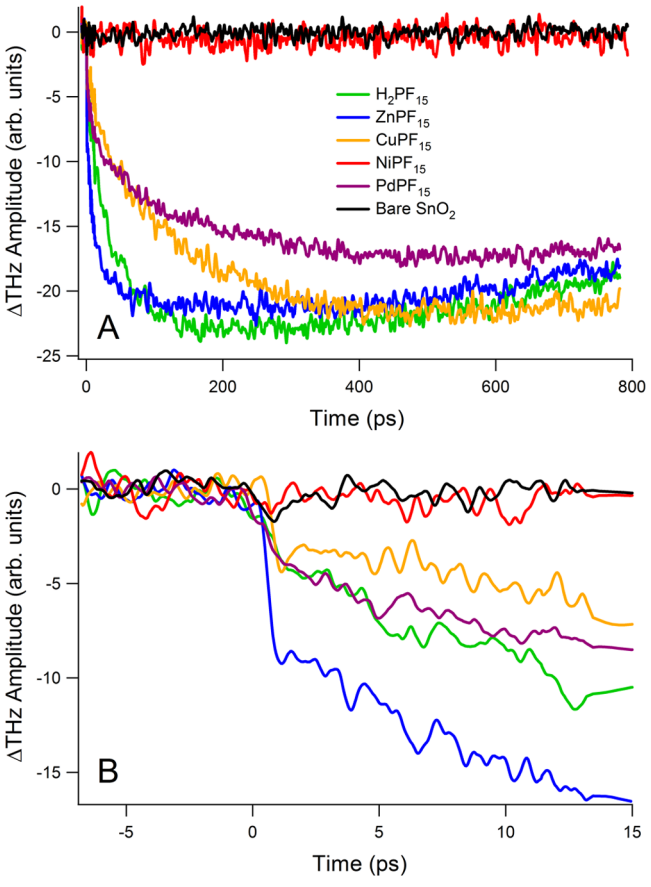

Figure 5. Electron injection dynamics into SnO_2 with 400 nm excitation measured from (A) −5 to 800 ps and (B) −5 to 15 ps. Photoexcitation occurs at 0 ps. The same line colors are used in parts A and B.

scale is consistent with other studies which have reported sub-picosecond injection times for similar pentafluorophenyl porphyrin sensitizers on TiO_2.[6,34] Both the lifetimes and energetics of the dye's excited states relative to the TiO_2 conduction band edge influence electron injection. The S_2 state of $ZnPF_{15}$ has a lifetime of roughly 2 ps,[52,53] which is relatively long-lived compared to the electron injection time scale. As seen in Figure 3 and discussed previously, the S_1 reduction potential of $ZnPF_{15}$ is higher in energy than the TiO_2 band edge, whereas the reduction potentials of the other dyes are either nearly isoenergetic with or positive of the conduction band edge. Thus, significant electron injection is observed only for $ZnPF_{15}$ because it has a relatively long S_2 excited state lifetime and an S_1 state energy slightly above the conduction band minimum.

A small amount of electron injection is also observed when using $CuPF_{15}$ and H_2PF_{15} as sensitizers. Since the S_2 state is the only excited state for H_2PF_{15} higher in energy than the TiO_2 conduction band, the observed electron injection must come from this state. In the case of $CuPF_{15}$, electron injection is unlikely to originate from the S_2 state as the S_2 state lifetimes of copper porphyrins are typically less than 100 fs.[54] Given that the $^2S_1$ state for $CuPF_{15}$ lies slightly above the conduction band edge of TiO_2, electron injection from it is possible. Although similar reasoning could be employed for $NiPF_{15}$, both the S_1 and S_2 lifetimes of Ni porphyrins typically range from 100 to 350 fs,[55,56] and the lack of injection from $NiPF_{15}$ is consistent with these short lifetimes.

SnO_2. The conduction band edge reduction potential of SnO_2 is ~0.5 V positive of the conduction band edge of TiO_2.[57,58] Therefore, electron injection from the S_1 state of all of the sensitizers is thermodynamically possible and, as seen in Figure 5, is indeed observed for all sensitizers reported here except $NiPF_{15}$. Electron injection into SnO_2 is significantly slower than that into TiO_2 and continues for tens to hundreds of picoseconds after photoexcitation. A similar trend has been observed previously by other researchers who attribute this decrease in rate to a decrease in the density of states in the conduction band of SnO_2 as compared to TiO_2.[17,21,26,59]

Electron injection dynamics were quantified by fitting eq 2 to the measured data (excluding $NiPF_{15}$) using the Levenberg–Marquardt nonlinear least-squares fitting algorithm.

$$\Delta THz = \Delta THz_0[A_1(e^{-t/\tau_1} - 1) + A_2(e^{-t/\tau_2} - 1) + (1 - e^{-t/\tau_r})] \quad (2)$$

Electron injection is modeled as a double exponential with time constants τ_1 and τ_2 and relative amplitudes A_1 and A_2 (where $A_1 + A_2 = 1$), and the $1 - e^{-t/\tau_r}$ term accounts for recombination. The measured change in THz amplitude as a function of pump/probe delay time is denoted ΔTHz, and ΔTHz_0 is a scaling factor that indicates the relative injection efficiency. (ΔTHz and ΔTHz_0 have the same arbitrary units, and no further scaling of individual traces is performed.) Thus, the change in THz amplitude is a measure of the amount of charge injection from a particular photoexcited chromophore. If τ_r is long compared to τ_1 and τ_2, then ΔTHz_0 represents the maximum change in THz amplitude. A global fit of all four data sets was performed in which τ_r was a shared parameter because loss of mobility over this short injection time scale is due mainly to trapping in the SnO_2 nanoparticles and not to reduction of the sensitizer cation. The results are shown in Table 3.

For all of the porphyrins studied, the values of ΔTHz_0 are similar. The slightly lower value for $PdPF_{15}$ is due to its lower absorbance at 400 nm (see Figure S1). These ΔTHz_0 values quantify the overall trend seen in Figure 5A: The photoinjected electron density is slightly lower for PdPF15 than for the other three dyes.

dx.doi.org/10.1021/jp406734t | J. Phys. Chem. C 2013, 117, 21662−21670

Table 3. Fitted Parameters of eq 2

porphyrin	ΔTHz_0 (arb. units)	A_1	τ_1 (ps)	A_2	τ_2 (ps)	τ_r (ns)
H_2PF_{15}	24	0.19	1.20	0.81	37.4	4.5
$ZnPF_{15}$	23	0.38	0.44	0.62	18.1	4.5
$CuPF_{15}$	26	0.30	10.5	0.70	180	4.5
$PdPF_{15}$	21	0.44	5.14	0.56	197	4.5

In contrast, the time constants for electron injection, τ_1 and τ_2, span an order of magnitude for the different dyes. While electron injection is completed within 20 ps for $ZnPF_{15}$ and within 40 ps for H_2PF_{15}, it continues for about 200 ps for both $CuPF_{15}$ and $PdPF_{15}$. Overall, the ordering of electron injection rates is $ZnPF_{15} > H_2PF_{15} > PdPF_{15} \approx CuPF_{15}$. Although many researchers have observed a decrease in electron injection rate with increasing reduction potential,[15,20,60] this relationship is not found in the results shown in Table 3. Specifically, if only the estimated reduction potentials of the S_1 states are considered, then the rates would be in the order of $ZnPF_{15} > CuPF_{15} > PdPF_{15} > H_2PF_{15}$. This lack of correlation indicates that factors in addition to the photoelectrochemical properties of the porphyrin singlet states determine the rate of electron injection.

The TRTS results for PF_{15}-sensitized SnO_2 can be rationalized by considering the kinetic competition between electron injection from the dyes and relaxation of the porphyrin excited states via other processes. If the rate of electron injection from a particular excited state is greater than the rate of deactivation, then electron injection may occur. If the converse is true, electron injection is disfavored. In the TRTS experiments described previously, the photoexcitation energy was 3.1 eV (400 nm), which is slightly greater than the $S_0 - S_2$ transition energy for all of the porphyrins used in this study. The presence of as many as three porphyrin excited states above the SnO_2 conduction band edge (see Figures 1B and 3) allows for many different electron injection pathways.

Soret (S_2) excitations can lead to internal conversion to the S_1 state which may be followed by intersystem crossing to a manifold of triplet states.[29] As has been observed for other sensitizers with multiple accessible excited states,[12,16,23,59] electron injection from any of these states can occur as long as they are higher in energy than the conduction band edge and exhibit adequate electronic coupling to conduction band states. As discussed previously, all of the S_1 and S_2 states of the porphyrins examined here are higher in energy than the SnO_2 conduction band edge, and many of the T_1 states are estimated to be higher in energy as well (Figure 3).[16,23,59,61]

In the remainder of the discussion, injection dynamics of the PF_{15} porphyrins are considered in the context of their classification as either fluorescent, phosphorescent, luminescent, or radiationless.[29,31] In all cases, electron injection rates are assumed to decrease for lower-lying excited states, as observed previously for other sensitizers.[16,23,59,61] Excited-state lifetimes are taken from the literature for the more widely studied meso-tetrakis(pentafluorophenyl)porphyrin (PF_{20}), in which all four of the meso positions are substituted with pentafluorophenyl groups. In some cases where PF_{20} data are unavailable, meso-tetraphenylporphyrin (TPP) data are used, since fluorination of the phenyl rings should not significantly alter excited state lifetimes.[62]

Fluorescent. Zn and free-base porphyrins are classified as fluorescent.[29,31] In addition, Zn porphyrins have relatively long-lived S_2 states (up to 2 ps) which are capable of participating in energy transfer before undergoing internal conversion,[53,63−66] and the S_2 lifetime of $ZnPF_{20}$ in ethanol is 0.19 ps.[52] The time constant of the fast electron injection component, τ_1, for $ZnPF_{15}$ is 0.44 ps, which is slightly longer than the lifetime of $ZnPF_{20}$. Because the instrument response time of the TRTS apparatus is ∼400 fs,[39,40] τ_1 represents an upper limit for electron injection, and the actual value could be closer to the $ZnPF_{20}$ S_2 lifetime. Therefore, this fast component corresponds to injection from the S_2 state. Since S_1 lifetimes for Zn porphyrins are generally on the order of nanoseconds,[52,62,63] and the slow injection component observed for $ZnPF_{15}$ is 18.1 ps, this slower component is attributed to electron injection from the S_1 state. Furthermore, τ_2 for $ZnPF_{15}$ is the actual electron injection time constant, unlike τ_1 which is a measure of the excited state lifetime.

A similar rationale is applied to the data for H_2PF_{15}, for which τ_1 = 1.20 ps and τ_2 = 37.4 ps. Reported lifetimes of the free-base S_2 state are typically less than 100 fs,[53,67] which is seemingly inconsistent with the observed 1.20 ps electron injection time of H_2PF_{15}. However, it is known that a small energy gap between the Q_y and B bands in free-base porphyrins leads to a strong coupling between them, as manifested in an enhanced Q_y band intensity relative to the Q_x band, and this coupling promotes the rapid deactivation of the S_2 state.[29] As seen in the UV−vis spectra in Figure 2B, the enhancement of the Q_y band at 500 nm relative to the Q_x band at 590 nm is less pronounced when H_2PF_{15} is bound to SnO_2 compared to solutions in dichloromethane. Thus, the coupling is not as strong when bound to SnO_2, and the measured 1.20 ps electron injection time is the lifetime of the S_2 state. Lifetimes of the H_2PF_{20} S_1 states range from 9.8 to 11.2 ns.[62,68,69] Accordingly, the observed 37.4 ps component of electron injection from H_2PF_{15} is the time constant for injection from the S_1 state.

Phosphorescent. Pd porphyrins are typically classified as phosphorescent.[29,31] Electron injection from $PdPF_{15}$ is much slower than that from H_2PF_{15} and $ZnPF_{15}$, and the values of τ_1 and τ_2 for $PdPF_{15}$ are 5.14 and 197 ps, respectively. For Pd porphyrins, the lifetimes of porphyrin S_1 and S_2 states are shortened due to spin−orbit coupling and the heavy atom effect. Instead of fluorescence from S_1, intersystem crossing to a triplet state T_1 occurs. As compared to the nanosecond S_1 lifetimes of Zn and free-base porphyrins, Pd porphyrin S_1 lifetimes are much shorter and range from 13 to 20 ps.[29] Triplet states, however, are much longer lived. For PdTPP, T_1 lifetimes on the order of microseconds have been reported.[29,70,71] Therefore, the measured τ_1 time constant is actually the $S_1 \rightarrow T_1$ intersystem crossing time constant. Since τ_2 is orders of magnitude smaller than the triplet state lifetime, it accurately represents the electron injection time constant from the T_1 state.

Luminescent. The emission from Cu(II) porphyrins cannot be considered either purely fluorescent or phosphorescent, and thus, they are classified as luminescent.[29,31] Because they are paramagnetic and have an unpaired electron in the $d_{x^2-y^2}$ orbital of the Cu(II) cation, their first excited triplet states (T_1) are split into a tripdoublet ($^2T_1$) and tripquartet ($^4T_1$), which are separated by 200−700 cm^{-1} depending on the substituents.[29] For $CuPF_{20}$, this splitting is 270 cm^{-1},[72] and intersystem crossing from the $^2S_1$ state to the ^2T state occurs in less than 350 fs.[73] Following intersystem crossing, an equilibrium is established between the ^2T and ^4T states.[29] Overall luminescence lifetimes of copper porphyrins range from 10 to 300 ns,[43,44,74] and the luminescence lifetime of $CuPF_{20}$ in

dx.doi.org/10.1021/jp406734t | J. Phys. Chem. C 2013, 117, 21662−21670

dichloromethane is 155 ns.[43] Cu porphyrins also exhibit (π, d) ligand-to-metal charge transfer (LMCT) states that lie close in energy to the triplet manifold.[29,75,76] The position of the LMCT state relative to the ^{2}T and ^{4}T states can vary with different ring substituents and is between the ^{2}T and ^{4}T states for CuTPP.[77]

$CuPF_{15}$ exhibits comparatively slow electron injection dynamics into SnO_2 (τ_1 = 10.5 ps and τ_2 = 180 ps). Assigning the two time constants to a particular state is more difficult in this case due to the increased number of possible excited states. A LMCT state can be ruled out, since (π, d) LMCT states involve the transfer of electrons from the porphyrin's ligands to the central metal ion and would quench electron injection. Given that the faster injection time constant in $CuPF_{15}$ is near that of the singlet state of $PdPF_{15}$ and the slower one is close to that from the triplet state of $PdPF_{15}$, τ_1 is assigned to the lifetime of a singdoublet ($^2S_1$) state of $CuPF_{15}$ and τ_2 to the injection time constant from its tripdoublet ($^2T_1$) state.

Radiationless. Electron injection was not observed for $NiPF_{15}$ bound to SnO_2 even though the reduction potential of its S_1 state lies about 0.5 eV negative of the conduction band edge of SnO_2. A significant difference between Ni porphyrins and the others is that they are radiationless and are known to have sub-picosecond S_1 and S_2 excited state lifetimes due to relaxation into empty d orbitals on the Ni(II) cation (which has a d^8 configuration).[55,56] Furthermore, these d states are highly localized on the Ni atom and lack electronic coupling to the SnO_2 conduction band. As a result, electron injection does not occur.

CONCLUSION

Electron-injection dynamics have been investigated using TRTS for a selection of high potential porphyrin dyes bound to TiO_2 and SnO_2 nanoparticles. Electron injection into TiO_2, or lack thereof, is determined by the energetic positioning of the singlet excited state of the dye molecule relative to the metal oxide conduction band edge. Because $ZnPF_{15}$ is the only sensitizer studied here with an S_1 state higher in energy than the TiO_2 conduction band, it is the only sensitizer to demonstrate significant electron injection. Given that the TiO_2 conduction band is unfavorably positioned with respect to the sensitizer excited state, these results suggest that TiO_2 may not be the best choice of semiconductor for these high-potential porphyrin sensitizers.

For SnO_2, all of the sensitizers studied in this report have excited states higher in energy than the SnO_2 conduction band edge. Accordingly, all of the porphyrins inject electrons upon photoexcitation except for $NiPF_{15}$. Changing the central substituent of the porphyrin ring changes the photoluminescent properties of the dye, leading to different pathways of excited state deactivation (fluorescence, phosphorescence, luminescence, or radiationless decay) and resulting in a range of excited state lifetimes. Since electron injection competes with this deactivation, it is strongly influenced by the identity of the central substituent. Therefore, the electron injection time constants obtained can be either indicators of the excited state lifetime or the actual electron injection time scale. For the biphasic dynamics observed, the shorter time constant represents the lifetime of a higher lying state, and the longer one is an intrinsic electron injection time constant for the lower lying state.

ASSOCIATED CONTENT

Supporting Information

Synthesis and characterization, additional UV−vis and emission spectra, cyclic voltammograms, and electrochemical values. This material is available free of charge via the Internet at http://pubs.acs.org.

AUTHOR INFORMATION

Corresponding Authors

*E-mail: gary.brudvig@yale.edu.

*E-mail: charles.schmuttenmaer@yale.edu.

Present Address

†G.F.M.: Joint Center for Artificial Photosynthesis (JCAP), Physical Biosciences division, Lawrence Berkeley National Laboratory, Berkeley, California 94720, United States.

Notes

The authors declare no competing financial interest.

ACKNOWLEDGMENTS

This work was supported by the Office of Basic Energy Sciences of the U.S. Department of Energy (DE-FG02-07ER15909) and the Camille & Henry Dreyfus Foundation.

REFERENCES

(1) O'Regan, B.; Grätzel, M. A Low-Cost, High-Efficiency Solar-Cell Based on Dye-Sensitized Colloidal TiO_2 Films. *Nature* **1991**, *353*, 737−740.

(2) Hagfeldt, A.; Boschloo, G.; Sun, L. C.; Kloo, L.; Pettersson, H. Dye-Sensitized Solar Cells. *Chem. Rev.* **2010**, *110*, 6595−6663.

(3) Moore, G. F.; Brudvig, G. W.; Langer, J. S. Energy Conversion in Photosynthesis: A Paradigm for Solar Fuel Production. *Annu. Rev. Cond. Mat. Phys.* **2011**, *2*, 303−327.

(4) Blankenship, R. E.; Tiede, D. M.; Barber, J.; Brudvig, G. W.; Fleming, G.; Ghirardi, M.; Gunner, M. R.; Junge, W.; Kramer, D. M.; Melis, A.; et al. Comparing Photosynthetic and Photovoltaic Efficiencies and Recognizing the Potential for Improvement. *Science* **2011**, *332*, 805−809.

(5) Hammarström, L.; Winkler, J. R.; Gray, H. B.; Styring, S. Shedding Light on Solar Fuel Efficiencies. *Science* **2011**, *333*, 288−288.

(6) Moore, G. F.; Blakemore, J. D.; Milot, R. L.; Hull, J. F.; Song, H. E.; Cai, L.; Schmuttenmaer, C. A.; Crabtree, R. H.; Brudvig, G. W. A Visible Light Water-Splitting Cell with a Photoanode Formed by Codeposition of a High-Potential Porphyrin and an Iridium Water-Oxidation Catalyst. *Energy Environ. Sci.* **2011**, *4*, 2389−2392.

(7) Brimblecombe, R.; Koo, A.; Dismukes, G. C.; Swiegers, G. F.; Spiccia, L. Solar Driven Water Oxidation by a Bioinspired Manganese Molecular Catalyst. *J. Am. Chem. Soc.* **2010**, *132*, 2892−2894.

(8) Li, L.; Duan, L. L.; Xu, Y. H.; Gorlov, M.; Hagfeldt, A.; Sun, L. C. A Photoelectrochemical Device for Visible Light Driven Water Splitting by a Molecular Ruthenium Catalyst Assembled on Dye-Sensitized Nanostructured TiO_2. *Chem. Commun.* **2010**, *46*, 7307−7309.

(9) Youngblood, W. J.; Lee, S. H. A.; Kobayashi, Y.; Hernandez-Pagan, E. A.; Hoertz, P. G.; Moore, T. A.; Moore, A. L.; Gust, D.; Mallouk, T. E. Photoassisted Overall Water Splitting in a Visible Light-Absorbing Dye-Sensitized Photoelectrochemical Cell. *J. Am. Chem. Soc.* **2009**, *131*, 926−927.

(10) Young, K. J.; Martini, L. A.; Milot, R. L.; Snoeberger, R. C., III; Batista, V. S.; Schmuttenmaer, C. A.; Crabtree, R. H.; Brudvig, G. W. Light-Driven Water Oxidation for Solar Fuels. *Coord. Chem. Rev.* **2012**, *256*, 2503−2520.

(11) Swierk, J. R.; Mallouk, T. E. Design and Development of Photoanodes for Water-Splitting Dye-Sensitized Photoelectrochemical Cells. *Chem. Soc. Rev.* **2013**, *42*, 2357−2387.

(12) Listorti, A.; O'Regan, B.; Durrant, J. R. Electron Transfer Dynamics in Dye-Sensitized Solar Cells. *Chem. Mater.* **2011**, *23*, 3381−3399.
(13) Li, G. H.; Richter, C. P.; Milot, R. L.; Cai, L.; Schmuttenmaer, C. A.; Crabtree, R. H.; Brudvig, G. W.; Batista, V. S. Synergistic Effect Between Anatase and Rutile TiO_2 Nanoparticles in Dye-Sensitized Solar Cells. *Dalton Trans.* **2009**, 10078−10085.
(14) Koops, S. E.; O'Regan, B. C.; Barnes, P. R.; Durrant, J. R. Parameters Influencing the Efficiency of Electron Injection in Dye-Sensitized Solar Cells. *J. Am. Chem. Soc.* **2009**, *131*, 4808−4818.
(15) Dos Santos, T.; Morandeira, A.; Koops, S.; Mozer, A. J.; Tsekouras, G.; Dong, Y.; Wagner, P.; Wallace, G.; Earles, J. C.; Gordon, K. C.; et al. Injection Limitations in a Series of Porphyrin Dye-Sensitized Solar Cells. *J. Phys. Chem. C* **2010**, *114*, 3276−3279.
(16) Listorti, A.; Lopez-Duarte, I.; Martinez-Diaz, M. V.; Torres, T.; DosSantos, T.; Barnes, P. R. F.; Durrant, J. R. Zn(II) versus Ru(II) Phthalocyanine-Sensitised Solar Cells. A Comparison Between Singlet and Triplet Electron Injectors. *Energy Environ. Sci.* **2010**, *3*, 1573−1579.
(17) Tiwana, P.; Docampo, P.; Johnston, M. B.; Snaith, H. J.; Herz, L. M. Electron Mobility and Injection Dynamics in Mesoporous ZnO, SnO_2, and TiO_2 Films Used in Dye-Sensitized Solar Cells. *ACS Nano* **2011**, *5*, 5158−5166.
(18) Song, W. J.; Brennaman, M. K.; Concepcion, J. J.; Jurss, J. W.; Hoertz, P. C.; Luo, H. L.; Chen, C. C.; Hanson, K.; Meyer, T. J. Interfacial Electron Transfer Dynamics for $[Ru(bpy)_2((4,4'\text{-}PO_3H_2)_2(bpy)]^{2+}$ Sensitized TiO_2 in a Dye-Sensitized Photoelectrosynthesis Cell: Factors Influencing Efficiency and Dynamics. *J. Phys. Chem. C* **2011**, *115*, 7081−7091.
(19) Heimer, T. A.; Heilweil, E. J.; Bignozzi, C. A.; Meyer, G. J. Electron Injection, Recombination, and Halide Oxidation Dynamics at Dye-Sensitized Metal Oxide Interfaces. *J. Phys. Chem. A* **2000**, *104*, 4256−4262.
(20) Asbury, J. B.; Anderson, N. A.; Hao, E. C.; Ai, X.; Lian, T. Q. Parameters Affecting Electron Injection Dynamics from Ruthenium Dyes to Titanium Dioxide Nanocrystalline Thin Films. *J. Phys. Chem. B* **2003**, *107*, 7376−7386.
(21) Furube, A.; Murai, M.; Watanabe, S.; Hara, K.; Katoh, R.; Tachiya, M. Near-IR Transient Absorption Study on Ultrafast Electron-Injection Dynamics from a Ru-complex Dye into Nanocrystalline In_2O_3 Thin Films: Comparison with SnO_2,ZnO, and TiO_2 Films. *J. Photochem. Photobiol., A* **2006**, *182*, 273−279.
(22) Haque, S. A.; Palomares, E.; Cho, B. M.; Green, A. N. M.; Hirata, N.; Klug, D. R.; Durrant, J. R. Charge Separation versus Recombination in Dye-Sensitized Nanocrystalline Solar Cells: the Minimization of Kinetic Redundancy. *J. Am. Chem. Soc.* **2005**, *127*, 3456−3462.
(23) Kallioinen, J.; Benko, G.; Sundstrom, V.; Korppi-Tommola, J. E. I.; Yartsev, A. P. Electron Transfer from the Singlet and Triplet Excited States of $Ru(dcbpy)_2(NCS)_2$ into Nanocrystalline TiO_2 Thin Films. *J. Phys. Chem. B* **2002**, *106*, 4396−4404.
(24) Turner, G. M.; Beard, M. C.; Schmuttenmaer, C. A. Carrier Localization and Cooling in Dye-Sensitized Nanocrystalline Titanium Dioxide. *J. Phys. Chem. B* **2002**, *106*, 11716−11719.
(25) Baxter, J. B.; Schmuttenmaer, C. A. Conductivity of ZnO Nanowires, Nanoparticles, and Thin Films Using Time-Resolved Terahertz Spectroscopy. *J. Phys. Chem. B* **2006**, *110*, 25229−25239.
(26) Pijpers, J. J. H.; Ulbricht, R.; Derossi, S.; Reek, J. N. H.; Bonn, M. Picosecond Electron Injection Dynamics in Dye-Sensitized Oxides in the Presence of Electrolyte. *J. Phys. Chem. C* **2011**, *115*, 2578−2584.
(27) Němec, H.; Rochford, J.; Taratula, O.; Galoppini, E.; Kužel, P.; Polívka, T.; Yartsev, A.; Sundstrom, V. Influence of the Electron-Cation Interaction on Electron Mobility in Dye-Sensitized ZnO and TiO_2 Nanocrystals: A Study Using Ultrafast Terahertz Spectroscopy. *Phys. Rev. Lett.* **2010**, *104*, 197401.
(28) Tiwana, P.; Parkinson, P.; Johnston, M. B.; Snaith, H. J.; Herz, L. M. Ultrafast Terahertz Conductivity Dynamics in Mesoporous TiO_2: Influence of Dye Sensitization and Surface Treatment in Solid-State Dye-Sensitized Solar Cells. *J. Phys. Chem. C* **2010**, *114*, 1365−1371.
(29) Kalyanasundaram, K. *Photochemistry of Polypyridine and Porphyrin Complexes*; Acedemic Press: New York, 1992.
(30) Panda, M. K.; Ladomenou, K.; Coutsolelos, A. G. Porphyrins in Bio-inspired Transformations: Light-Harvesting to Solar Cell. *Coord. Chem. Rev.* **2012**, *256*, 2601−2627.
(31) Gouterman, M. Optical Spectra and Electronic Structure of Porphyrins. In *The Porphyrins*; Dolphin, D., Ed.; Academic Press: New York, 1978; Vol. *III*.
(32) Okura, I. *Photosensitization of Porphyrins and Phthalocyanines*; Kodansha, Ltd. and Gordon and Breach Science Publishers: Tokyo, Japan, 2000.
(33) Yella, A.; Lee, H. W.; Tsao, H. N.; Yi, C. Y.; Chandiran, A. K.; Nazeeruddin, M. K.; Diau, E. W. G.; Yeh, C. Y.; Zakeeruddin, S. M.; Grätzel, M. Porphyrin-Sensitized Solar Cells with Cobalt (II/III)-Based Redox Electrolyte Exceed 12% Efficiency. *Science* **2011**, *334*, 629−634.
(34) Moore, G. F.; Konezny, S. J.; Song, H. E.; Milot, R. L.; Blakemore, J. D.; Lee, M. L.; Batista, V. S.; Schmuttenmaer, C. A.; Crabtree, R. H.; Brudvig, G. W. Bioinspired High-Potential Porphyrin Photoanodes. *J. Phys. Chem. C* **2012**, *116*, 4892−4902.
(35) Nango, M.; Iida, K.; Yamaguchi, M.; Yamashita, K.; Tsuda, K.; Mizusawa, A.; Miyake, T.; Masuda, A.; Yoshinaga, J. Transmembrane Electron Transfer as Catalyzed by Phospholipid-Linked Manganese Porphyrins. *Langmuir* **1996**, *12*, 1981−1988.
(36) Adler, A. D.; Longo, F. R.; Kampas, F.; Kim, J. On Preparation of Metalloporphyrins. *J. Inorg. Nucl. Chem.* **1970**, *32*, 2443−2445.
(37) Mills, A.; LeHunte, S. An Overview of Semiconductor Photocatalysis. *J. Photochem. Photobiol., A* **1997**, *108*, 1−35.
(38) Sawyer, D. T.; Sobkowiak, A.; Roberts, J. L. *Electrochemistry for Chemists*, 2nd ed.; Wiley: New York, 1995.
(39) Beard, M. C.; Turner, G. M.; Schmuttenmaer, C. A. Transient Photoconductivity in GaAs as Measured by Time-Resolved Terahertz Spectroscopy. *Phys. Rev. B* **2000**, *62*, 15764−15777.
(40) Beard, M. C.; Turner, G. M.; Schmuttenmaer, C. A. Subpicosecond Carrier Dynamics in Low-Temperature Grown GaAs as Measured by Time-Resolved Terahertz Spectroscopy. *J. Appl. Phys.* **2001**, *90*, 5915−5923.
(41) Khairutdinov, R. F.; Serpone, N. Photoluminescence and Transient Spectroscopy of Free Base Porphyrin Aggregates. *J. Phys. Chem. B* **1999**, *103*, 761−769.
(42) Smith, B. E.; Gouterman, M. Quartet Luminescence from Copper Porphyrins. *Chem. Phys. Lett.* **1968**, *2*, 517−519.
(43) Cunningham, K. L.; McNett, K. M.; Pierce, R. A.; Davis, K. A.; Harris, H. H.; Falck, D. M.; McMillin, D. R. EPR Spectra, Luminescence Data, and Radiationless Decay Processes of Copper(II) Porphyrins. *Inorg. Chem.* **1997**, *36*, 608−613.
(44) Asano, M.; Kaizu, Y.; Kobayashi, H. The Lowest Excited-States of Copper Porphyrins. *J. Chem. Phys.* **1988**, *89*, 6567−6576.
(45) Moore, G. F.; Hambourger, M.; Gervaldo, M.; Poluektov, O. G.; Rajh, T.; Gust, D.; Moore, T. A.; Moore, A. L. A Bioinspired Construct that Mimics the Proton Coupled Electron Transfer Between $P680^+$ and the Tyr_Z-His190 Pair of Photosystem II. *J. Am. Chem. Soc.* **2008**, *130*, 10466−10467.
(46) Moore, G. F.; Hambourger, M.; Kodis, G.; Michl, W.; Gust, D.; Moore, T. A.; Moore, A. L. Effects of Protonation State on a Tyrosine-Histidine Bioinspired Redox Mediator. *J. Phys. Chem. B* **2010**, *114*, 14450−14457.
(47) Rehm, D.; Weller, A. Kinetics and Mechanics of Electron Transfer During Fluorescence Quenching in Acetonitrile. *Ber. Bunsen-Ges.* **1969**, *73*, 834−839.
(48) Rehm, D.; Weller, A. Kinetics of Fluorescence Quenching by Electron and H-Atom Transfer. *Isr. J. Chem.* **1970**, *8*, 259−271.
(49) McNamara, W. R.; Snoeberger, R. C.; Li, G.; Schleicher, J. M.; Cady, C. W.; Poyatos, M.; Schmuttenmaer, C. A.; Crabtree, R. H.; Brudvig, G. W.; Batista, V. S. Acetylacetonate Anchors for Robust Functionalization of TiO_2 Nanoparticles with Mn(II)-Terpyridine Complexes. *J. Am. Chem. Soc.* **2008**, *130*, 14329−14338.

(50) Richter, C.; Schmuttenmaer, C. A. Exciton-like Trap States Limit Electron Mobility in TiO_2 Nanotubes. *Nat. Nanotechnol.* **2010**, *5*, 769−772.
(51) Ashcroft, N. W.; Mermin, N. D. *Solid State Physics*; Saunders College: Philadelphia, PA, 1976.
(52) Liu, X.; Yeow, E. K. L.; Velate, S.; Steer, R. P. Photophysics and Spectroscopy of the Higher Electronic States of Zinc Metalloporphyrins: A Theoretical and Experimental Study. *Phys. Chem. Chem. Phys.* **2006**, *8*, 1298−1309.
(53) Tripathy, U.; Kowalska, D.; Liu, X.; Velate, S.; Steer, R. P. Photophysics of Soret-excited Tetrapyrroles in Solution. I. Metalloporphyrins: MgTPP, ZnTPP, and CdTPP. *J. Phys. Chem. A* **2008**, *112*, 5824−5833.
(54) Yeon, K. Y.; Jeong, D.; Kim, S. K. Intrinsic Lifetimes of the Soret bands of the Free-Base Tetraphenylporphine (H_2TPP) and Cu(II)-TPP in the Condensed Phase. *Chem. Commun.* **2010**, *46*, 5572−5574.
(55) Rodriguez, J.; Holten, D. Ultrafast Vibrational Dynmaics of a Photoexcited Metalloporphyrin. *J. Chem. Phys.* **1989**, *91*, 3525−3531.
(56) Zhang, X. Y.; Wasinger, E. C.; Muresan, A. Z.; Attenkofer, K.; Jennings, G.; Lindsey, J. S.; Chen, L. X. Ultrafast Stimulated Emission and Structural Dynamics in Nickel Porphyrins. *J. Phys. Chem. A* **2007**, *111*, 11736−11742.
(57) Grätzel, M. Photoelectrochemical cells. *Nature* **2001**, *414*, 338−344.
(58) Rothenberger, G.; Fitzmaurice, D.; Grätzel, M. Optical Electrochemistry 3. Spectroscopy of Conduction-Band Electrons in Trasparent Metal-Oxide Semiconductor-Films - Optical Determination of the Flat-Band Potential of Colloidal Titanium-Dioxide Films. *J. Phys. Chem.* **1992**, *96*, 5983−5986.
(59) Ai, X.; Anderson, N. A.; Guo, J. C.; Lian, T. Q. Electron Injection Dynamics of Ru Polypyridyl Complexes on SnO_2 Nanocrystalline Thin Films. *J. Phys. Chem. B* **2005**, *109*, 7088−7094.
(60) Asbury, J. B.; Hao, E.; Wang, Y. Q.; Ghosh, H. N.; Lian, T. Q. Ultrafast Electron Transfer Dynamics from Molecular Adsorbates to Semiconductor Nanocrystalline Thin Films. *J. Phys. Chem. B* **2001**, *105*, 4545−4557.
(61) Koops, S. E.; Barnes, P. R. F.; O'Regan, B. C.; Durrant, J. R. Kinetic Competition in a Coumarin Dye-Sensitized Solar Cell: Injection and Recombination Limitations upon Device Performance. *J. Phys. Chem. C* **2010**, *114*, 8054−8061.
(62) Yang, S. I.; Seth, J.; Strachan, J. P.; Gentemann, S.; Kim, D.; Holten, D.; Lindsey, J. S.; Bocian, D. F. Ground and Excited State Electronic Properties of Halogenated Tetraarylporphyrins. Tuning the Building Blocks for Porphyrin-Based Photonic Devices. *J. Porphyrins Phthalocyanines* **1999**, *3*, 117−147.
(63) Lukaszewicz, A.; Karolczak, J.; Kowalska, D.; Maciejewski, A.; Ziolek, M.; Steer, R. P. Photophysical Processes in Electronic States of Zinc Tetraphenyl Porphyrin Accessed on One- and Two-Photon Excitation in the Soret Region. *Chem. Phys.* **2007**, *331*, 359−372.
(64) Hayes, R. T.; Walsh, C. J.; Wasielewski, M. R. Competitive Electron Transfer from the S_2 and S_1 Excited States of Zinc Meso-tetraphenylporphyrin to a Covalently Bound Pyromellitimide: Dependence on Donor-Acceptor Structure and Solvent. *J. Phys. Chem. A* **2004**, *108*, 2375−2381.
(65) Mataga, N.; Shibata, Y.; Chosrowjan, H.; Yoshida, N.; Osuka, A. Internal Conversion and Vibronic Relaxation from Higher Excited Electronic State of Porphyrins: Femtosecond Fluorescence Dynamics Studies. *J. Phys. Chem. B* **2000**, *104*, 4001−4004.
(66) Kiyosawa, K.; Shiraishi, N.; Shimada, T.; Masui, D.; Tachibana, H.; Takagi, S.; Ishitani, O.; Tryk, D. A.; Inoue, H. Electron Transfer from the Porphyrin S-2 State in a Zinc Porphyrin-Rhenium Bipyridyl Dyad having Carbon Dioxide Reduction Activity. *J. Phys. Chem. C* **2009**, *113*, 11667−11673.
(67) Baskin, J. S.; Yu, H. Z.; Zewail, A. H. Ultrafast Dynamics of Porphyrins in the Condensed Phase: I. Free Base Tetraphenylporphyrin. *J. Phys. Chem. A* **2002**, *106*, 9837−9844.
(68) Prashanthi, S.; Kumar, P. H.; Wang, L.; Perepogu, A. K.; Bangal, P. R. Reductive Fluorescence Quenching of the Photoexcited Free Base meso-Tetrakis (Pentafluorophenyl) Porphyrin by Amines. *J. Fluoresc.* **2010**, *20*, 571−580.
(69) Grancho, J. C. P.; Pereira, M. M.; Miguel, M. D.; Gonsalves, A. M. R.; Burrows, H. D. Synthesis, Spectra and Photophysics of Some Free Base Tetrafluoroalkyl and Tetrafluoroaryl Porphyrins with Potential Applications in Imaging. *Photochem. Photobiol.* **2002**, *75*, 249−256.
(70) Faure, S.; Stern, C.; Guilard, R.; Harvey, P. D. Synthesis and Photophysical Properties of Meso-substituted Bisporphyrins: Comparative Study of Phosphorescence Quenching for Dioxygen Sensing. *Inorg. Chem.* **2005**, *44*, 9232−9241.
(71) Rogers, J. E.; Nguyen, K. A.; Hufnagle, D. C.; McLean, D. G.; Su, W. J.; Gossett, K. M.; Burke, A. R.; Vinogradov, S. A.; Pachter, R.; Fleitz, P. A. Observation and Interpretation of Annulated Porphyrins: Studies on the Photophysical Properties of Meso-tetraphenylmetalloporphyrins. *J. Phys. Chem. A* **2003**, *107*, 11331−11339.
(72) Spellane, P. J.; Gouterman, M.; Antipas, A.; Kim, S.; Liu, Y. C. Prophyrins. 40. Electronic Spectra and 4-Orbital Energies of Free-Base, Zinc, Copper, and Palladium Tetrakis(perfluorophenyl)porphyrins. *Inorg. Chem.* **1980**, *19*, 386−391.
(73) Rodriguez, J.; Kirmaier, C.; Holten, D. Optical Properties of Metalloporphyrin Excited States. *J. Am. Chem. Soc.* **1989**, *111*, 6500−6506.
(74) Kim, D.; Holten, D.; Gouterman, M. Evidence from Picosecond Transient Absorption and Kinetic Studies of Charge-Transfer States in Copper(II) Porphyrins. *J. Am. Chem. Soc.* **1984**, *106*, 2793−2798.
(75) Jeoung, S. C.; Kim, D. H.; Cho, D. W.; Yoon, M. J. Time-Resolved Resonance Raman Spectroscopic Study on Copper(II) Porphyrins in Various Solvents - Solvent Effects on the Charge-Transfer States. *J. Phys. Chem.* **1995**, *99*, 5826−5833.
(76) Jeoung, S. C.; Takeuchi, S.; Tahara, T.; Kim, D. Ultrafast Decay Dynamics of Photoexcited Cu(II)(TMpy-P4) in Water Solvent. *Chem. Phys. Lett.* **1999**, *309*, 369−376.
(77) Yan, X. W.; Holten, D. Effects of Temperature and Solvent on Excite-State Deactivation of Copper(II) Octaethylporphyrin and Tetraphenylporphyrin - Relaxation via a Ring-to-Metal Charge-Transfer Excited-State. *J. Phys. Chem.* **1988**, *92*, 5982−5986.

Supporting Information for

Electron Injection Dynamics from Photoexcited Porphyrin Dyes into SnO_2 and TiO_2 Nanoparticles

Rebecca L. Milot, Gary F. Moore,[†] Robert H. Crabtree, Gary W. Brudvig, and Charles A. Schmuttenmaer**

Yale University, Department of Chemistry, 225 Prospect St., P.O. Box 208107, New Haven, CT 06520-8107, USA

charles.schmuttenmaer@yale.edu, gary.brudvig@yale.edu

Index

Synthesis and characterization.

5-(Pentafluorophenyl)dipyrromethane. A solution of pentafluorobenzaldehyde (2.0 mL, 16.2 mmol) in freshly distilled pyrrole (50 mL, 720 mmol) was degassed with a stream of argon for 20 min before adding trifluoroacetic acid (120 μL, 1.62 mmol). The mixture was stirred for 30 min at room temperature, diluted with CH_2Cl_2 (400 mL), and then washed with 0.1 M NaOH (400 mL). The organic phase was washed with water (400 mL) and dried over Na_2SO_4. Evaporation of the solvent at reduced pressure gave a brown oil. Unreacted pyrrole was removed under high vacuum, yielding a tacky solid that was flashed on a column of silica using a mixture of hexanes:ethylacetate:triethylamine (80:20:1) as the eluent. The product was recrystallized from dichloromethane/hexanes to yield 3.29 g of 5-(pentafluorophenyl)dipyrromethane as a white powder (65% yield). ^{1}H NMR (400 MHz, $CDCl_3$): δ 5.90 (1H, s, CH), 6.00 – 6.05 (2H, m, ArH), 6.14– 6.19 (2H, m, ArH), 6.71 – 6.75 (2H, m, ArH), 8.06 (2H, brs, NH); ^{19}F NMR (400 MHz, $CDCl_3$): δ -160.98 – -161.40 (2F, m, ArF), -155.71 (1F, t, J = 21.0 Hz, ArF), -141.43 (2F, brd, J = 20.7 Hz, ArF).

5-(4-carbomethoxyphenyl)-10,15,20-(pentafluorophenyl)porphyrin. A portion of 5-(pentafluorophenyl)dipyrromethane (1.25 g, 4.00 mmol), 4-carbomethoxybenzaldehyde (329 mg, 2.00 mmol) and pentafluorobenzaldehyde (247 μL, 2.00 mmol) in chloroform (400 mL) was purged for 20 minutes with argon before adding $BF_3(OEt_2)$ (530 μL of a 2.5 M stock solution in chloroform). After 24 h, 2,3-dichloro-5,6-dicyano-1,4-benzoquinone (DDQ) (700 mg, 3.08 mmol) was added and the mixture was stirred for an additional 24 h. The solvent was evaporated at reduced pressure and the residue was redissolved in bromobenzene. The solution was treated with a second portion of DDQ (700 mg, 3.08 mmol) and refluxed for 3 h. The solvent was removed at reduced pressure and the crude product was purified by column chromatography on silica using toluene as the eluent. (18% yield). ^{1}H NMR (400 MHz, $CDCl_3$): δ -2.87 (2H, s, NH), 4.13 (3H, s, CO_2CH_3), 8.31 (2H, d, J = 8.2 Hz, ArH), 8.48 (2H, d, J = 8.2 Hz, ArH), 8.83 (2H, d, J = 4.5Hz, βH), 8.87-8.94 (6H, m, βH); ^{19}F NMR (400 MHz, in $CDCl_3$): δ -161.61 – -161.34 (6F, m, ArF), -151.56 (2F, t, J = 20.7 Hz, ArF), -151.50 (1F, t, J = 20.7 Hz, ArF), -136.65 (4F, dd, J = 8.0 Hz, 22.9 Hz, ArF), -136.51 (2F, dd, J = 8.0 Hz, 22.9 Hz, ArF); MALDI-TOF-MS *m/z.* calcd. for $C_{46}H_{17}F_{15}N_4O_2$ 942.111, obsd. 942.115; UV-vis (CH_2Cl_2) 413, 507, 536, 583, 637 nm.

5-(4-Carboxyphenyl)-10,15,20-(pentafluorophenyl)porphyrin (PF15). A portion of 5-(4-carbomethoxyphenyl)-10,15,20-(pentafluorophenyl)porphyrin (100 mg, 0.11 mmol) was dissolved in a mixture of trifluoroacetic acid and conc. HCl (1:2, 80 mL) at 90 ^{o}C for 24 h. The reaction mixture was diluted with dichloromethane (80 mL), washed twice with an equal volume of water, and then neutralized with a saturated solution of aqueous sodium bicarbonate. The organic phase was dried over sodium sulfate, filtered, and the solvent removed at reduced pressure. The crude product was purified by column chromatography on silica using a gradient of 1% methanol in dichloromethane to 10% methanol in dichloromethane as the eluent to give 96 mg of the desired porphyrin (98% yield). ^{1}H NMR (400 MHz, $CDCl_3$): δ -2.86 (2H, s, NH), 8.38 (2H, d, J = 8.3 Hz, ArH), 8.60 (2H, d, J = 8.3 Hz, ArH), 8.87 (2H, brd, J = 4.3 Hz, βH), 8.88-8.89 (6H, brm, βH); ^{19}F NMR (400 MHz, in $CDCl_3$): δ -161.59 – -161.30 (6F, m, ArF), -151.51 (2F, t, J = 20.7 Hz, ArF), -151.46 (1F, t, J = 20.7 Hz, ArF), -136.64 (4F, dd, J = 8.0 Hz, 22.9 Hz, ArF), -136.51 (2F, dd, J = 8.0 Hz, 22.9 Hz, ArF); MALDI-TOF-MS *m/z.* calcd. for $C_{45}H_{15}F_{15}N_4O_2$ 928.096, obsd. 928.098.

Zinc 5-(4-carbomethoxyphenyl)-10,15,20-(pentafluorophenyl)porphyrin. $Zn(OAc_2)\cdot 2H_2O$ (82 mg, 0.37 mmol) was added to a solution of 5-(4-carbomethoxyphenyl)-10,15,20-(pentafluorophenyl)porphyrin (35 mg, 0.04 mmol) in a mixture of dichloromethane and methanol (80:20, 40 mL). After cooling to room temperature, the solution was diluted with dichloromethane (20 mL) and washed with water (70 mL), then a saturated solution of aqueous sodium bicarbonate (70

mL). The organic phase was dried over sodium sulfate, filtered, and the solvent evaporated at reduced pressure. The product was purified by column chromatography on silica using toluene as the eluent to give 37 mg of the desired porphyrin (99% yield). ^{1}H NMR (400 MHz, $CDCl_3$): δ 4.08 (3H, s, CO_2CH_3), 8.30 (2H, d, *J* = 8.2 Hz, ArH), 8.42 (2H, d, *J* = 8.2 Hz, ArH), 8.92 (2H, d, *J* = 4.4Hz, βH), 8.97-9.01 (6H, m, βH); ^{19}F NMR (400 MHz, in $CDCl_3$): δ -161.96 – -161.68 (6F, m, ArF), -152.18 (2F, t, *J* = 20.7 Hz, ArF), -152.12 (1F, t, *J* = 20.7 Hz, ArF), -136.93 (4F, dd, *J* = 8.0 Hz, 22.9 Hz, ArF), -136.82 (2F, dd, *J* = 8.0 Hz, 22.9 Hz, ArF); UV-vis (CH_2Cl_2) 415, 544, 578 nm.

Zinc 5-(4-carboxyphenyl)-10,15,20-(pentafluorophenyl)porphyrin (ZnPF15). $Zn(OAc_2)\cdot 2H_2O$ (83 mg, 0.38 mmol) was added to a solution of 5-(4-carboxyphenyl)-10,15,20-(pentafluorophenyl)porphyrin (35 mg, 0.04 mmol) in a mixture of dichloromethane and methanol (80:20, 40 mL). After stirring for 15 h, the solution was heated at reflux for 4 h. After cooling to room temperature, the solution was diluted with dichloromethane (20 mL) and washed with water (70 mL), then a saturated solution of aqueous sodium bicarbonate (70 mL). The organic phase was dried over sodium sulfate, filtered, and the solvent evaporated at reduced pressure. The product was purified by column chromatography on silica using 5% methanol in dichloromethane as the eluent to give 36 mg of the desired porphyrin (97% yield). ^{1}H NMR (400 MHz, $CDCl_3$): δ 8.37 (2H, d, *J* = 8.3 Hz, ArH), 8.54 (2H, d, *J* = 8.3 Hz, ArH), 8.95 (2H, d, *J* = 4.5Hz, βH), 8.98-9.07 (6H, m, βH); ^{19}F NMR (400 MHz, in $CDCl_3$): δ -161.91 – -161.61 (6F, m, ArF), -152.09 (2F, t, *J* = 20.7 Hz, ArF), -152.04 (1F, t, *J* = 20.7 Hz, ArF), -136.91 (4F, dd, *J* = 8.0 Hz, 22.9 Hz, ArF), -136.81 (2F, dd, *J* = 8.0 Hz, 22.9 Hz, ArF).

Palladium 5-(4-carbomethoxyphenyl)-10,15,20-(pentafluorophenyl)porphyrin. Palladium (II) chloride (66 mg, 0.37 mmol) was added to a solution 5-(4-carbomethoxyphenyl)-10,15,20-(pentafluorophenyl)porphyrin (35 mg, 0.04 mmol) in N,N-dimethylformamide (15 mL). The mixture was stirred for 7 h at reflux under an argon atmosphere. The solvent was removed under reduced pressure and the crude product was purified by column chromatography on silica using toluene as the eluent to give 35 mg of the desired porphyrin (90% yield). ^{1}H NMR (400 MHz, $CDCl_3$): δ 4.12 (3H, s, CO_2CH_3), 8.27 (2H, d, *J* = 8.5 Hz, ArH), 8.47 (2H, d, *J* = 8.5 Hz, ArH), 8.80 (2H, d, *J* = 4.7Hz, βH), 8.85-8.89 (6H, m, βH); ^{19}F NMR (400 MHz, in $CDCl_3$): δ -161.49 – -161.24 (6F, m, ArF), -151.51 (2F, t, *J* = 20.7 Hz, ArF), -151.45 (1F, t, *J* = 20.7 Hz, ArF), -136.93 (4F, dd, *J* = 8.0 Hz, 22.9 Hz, ArF), -136.39 (2F, dd, *J* = 8.0 Hz, 22.9 Hz, ArF); UV-vis (CH_2Cl_2) 410, 520, 553 nm.

Palladium 5-(4-carboxyphenyl)-10,15,20-(pentafluorophenyl)porphyrin (PdPF15). Palladium(II) chloride (67 mg, 0.38 mmol) was added to a solution of 5-(4-carboxyphenyl)-10,15,20-(pentafluorophenyl)porphyrin (35 mg, 0.04 mmol) in N,N-dimethylformamide (15 mL). The mixture was stirred for 7 h at reflux under an argon atmosphere. The solvent was removed under reduced pressure and the crude product was purified by column chromatography on silica using 5% methanol in dichloromethane as the eluent. To give 36 mg of the desired porphyrin (92% yield). ^{1}H NMR (400 MHz, $CDCl_3$): δ 8.26 (2H, d, *J* = 8.2 Hz, ArH), 8.50 (2H, d, *J* = 8.2 Hz, ArH), 8.75 (2H, d, *J* = 4.7Hz, βH), 8.79-8.82 (4H, m, βH) 8.83 (2H, d, *J* = 4.7 Hz, βH); ^{19}F NMR (400 MHz, in $CDCl_3$): δ -161.51 – -161.19 (6F, m, ArF), -151.52 (2F, t, *J* = 21.8 Hz, ArF), -151.41 (1F, t, *J* = 21.8 Hz, ArF), -136.42 (4F, dd, *J* = 8.0 Hz, 22.9 Hz, ArF), -136.58 (2F, dd, *J* = 8.0 Hz, 22.9 Hz, ArF).

Nickel 5-(4-carboxyphenyl)-10,15,20-(pentafluorophenyl)porphyrin (NiPF15). $Ni(OAc_2)\cdot 4H_2O$ (94 mg, 0.38 mmol) was added to a solution of 5-(4-carboxyphenyl)-10,15,20-(pentafluorophenyl)porphyrin (35 mg, 0.04 mmol) in N,N-dimethylformamide (25 mL). The mixture was stirred for 24 h at reflux under an argon atmosphere. The solvent was removed under reduced pressure and the crude product was purified by column chromatography on silica using 5% methanol

in dichloromethane as the eluent to give 33 mg of the desired porphyrin (89% yield). ^{1}H NMR (400 MHz, $CDCl_3$): δ 8.15 (2H, d, *J* = 8.2 Hz, ArH), 8.47 (2H, d, *J* = 8.2 Hz, ArH), 8.72 (2H, d, *J* = 4.8 Hz, βH), 8.74-8.79 (4H, m, βH) 8.81 (2H, d, *J* = 4.8 Hz, βH); ^{19}F NMR (400 MHz, in $CDCl_3$): δ -161.45 – -161.24 (6F, m, ArF), -151.62 (2F, t, *J* = 21.8 Hz, ArF), -151.57 (1F, t, *J* = 21.8 Hz, ArF), -136.78 (4F, dd, *J* = 8.0 Hz, 22.9 Hz, ArF), -136.63 (2F, dd, *J* = 8.0 Hz, 22.9 Hz, ArF); UV-vis (CH_2Cl_2) 406, 524, 557 nm.

Copper 5-(4-carboxyphenyl)-10,15,20-(pentafluorophenyl)porphyrin (CuPF15). $Cu(OAc_2)$ (68 mg, 0.38 mmol) was added to a solution of 5-(4-carboxyphenyl)-10,15,20-(pentafluorophenyl)porphyrin (35 mg, 0.04 mmol) in dichloromethane (40 mL). After stirring for 12 h, the solution was heated at reflux for 3 h. After cooling to room temperature, the solution was diluted with dichloromethane (20 mL) and washed with water (70 mL), then a saturated solution of aqueous sodium bicarbonate (70 mL). The organic phase was dried over sodium sulfate, filtered, and the solvent evaporated at reduced pressure. The product was purified by column chromatography on silica using 5% methanol in dichloromethane as the eluent to give 34 mg of the desired porphyrin (91% yield); UV-vis (CH_2Cl_2) 409, 535, 570 nm.

Figure S1. UV-vis and emission spectra. Left: normalized absorption (solid line) and emission (dashed line) spectra of PF_{15} methyl esters in dichloromethane. The wavelength of the highest energy Q-band transition was chosen for excitation to obtain the emission spectra. Due to low emission, the spectrum for $NiPF_{15}$ has been given the same scaling as that of $CuPF_{15}$. Right: absorption spectra of the PF_{15} methyl esters in dichloromethane (medium), for the PF_{15} dyes on the TiO_2 surface (light), and for the PF_{15} dyes on the SnO_2 surface (dark).

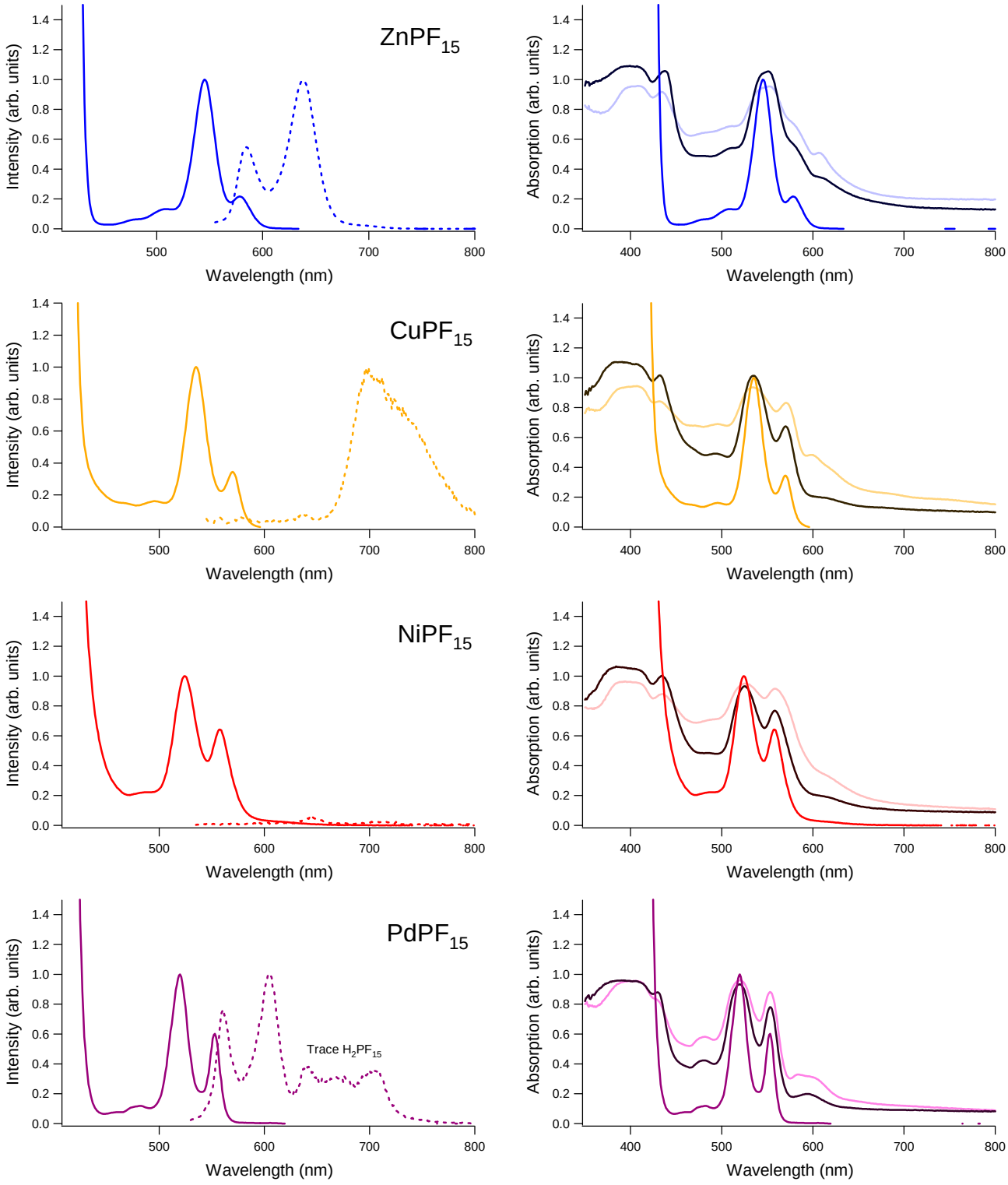

Figure S2. Unscaled emission spectra. Concentrations of all species have been approximately absorbance matched, and spectra have been divided into parts A and B to highlight order of magnitude differences in emission intensity.

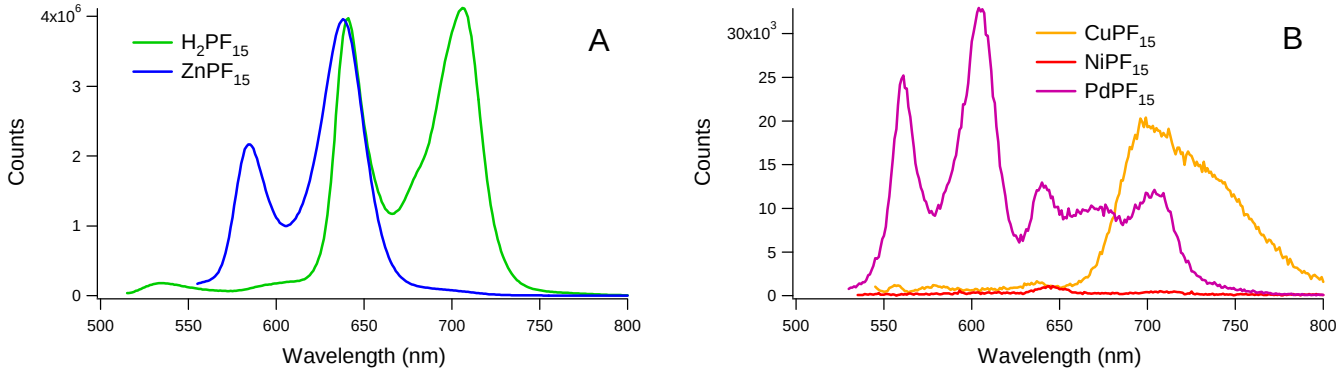

Figure S3. Cyclic voltammograms of the PF_{15} methyl esters. The electrolyte was 0.1 M tetrabutylammonium hexafluorophosphate in dichloromethane, and the scan rate was 100 mV/s. First and second oxidations are observed for H_2PF_{15}, $ZnPF_{15}$, and $CuPF_{15}$. Only the first oxidation is observed for $NiPF_{15}$ and $PdPF_{15}$ due to the limitations of the solvent window.

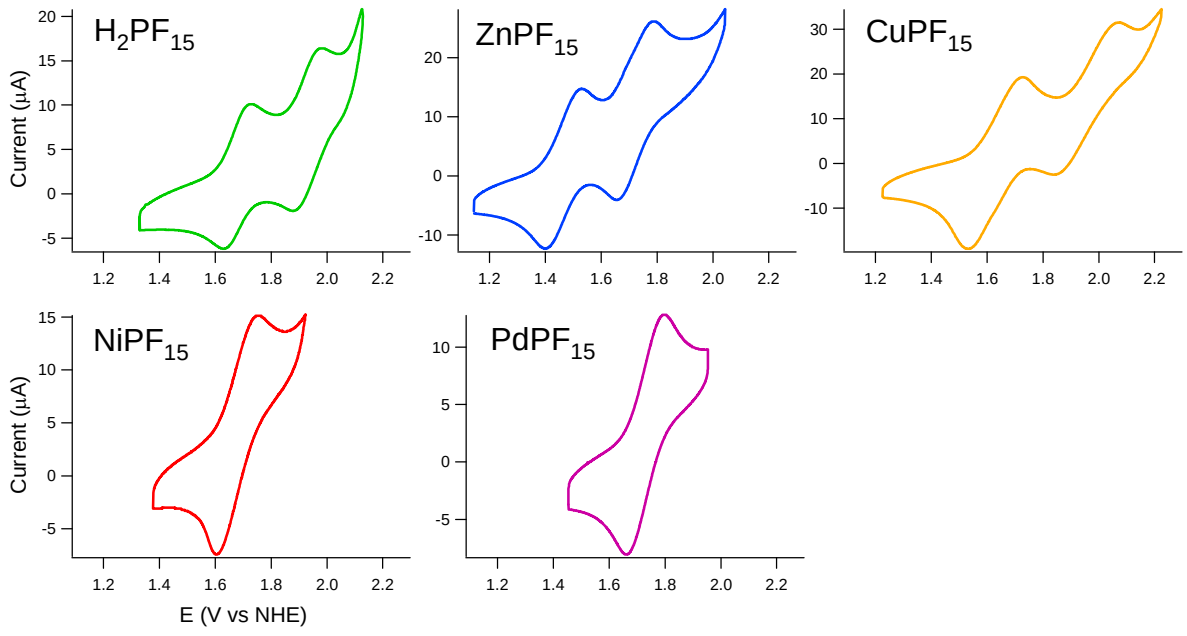

Table S1. Electrochemical values.

Porphyrin	P^+/P (V)[a]	$P^+/{}^3P^*$(V)[b]	$P^+/{}^1P_{(S1)}{}^*$(V)[c]	E^{00} (eV)	$P^+/{}^1P_{(S2)}{}^*$(V)[d]	E_{Soret} (eV)
H_2PF_{15}	1.68	0.18	-0.25	1.93	-1.33	3.01
$ZnPF_{15}$	1.47	-0.20	-0.66	1.47	-1.52	2.99
$CuPF_{15}$	1.63	-0.08	-0.55	2.10	-1.40	3.03
$NiPF_{15}$	1.68	–	-0.55	2.10	-1.37	3.05
$PdPF_{15}$	1.73	-0.03	-0.49	2.22	-1.29	3.02

[a] Ground state reduction potentials as determined by cyclic voltammetry.

[b] Triplet state reduction potentials estimated using electrochemical data for free-base, zinc, and palladium tetraphenylporphyrin (TPP) and the maximum value of triplet emission spectrum of CuTPP.

[c] S_1 state reduction potentials estimated by adding the E^{00} transition energies to the corresponding ground state potentials.

[d] S_2 state reduction potentials calculated using the energy of the Soret band maximum.